of needles of the α-phase and blocks of the new β-phase is produced; the two phases can be separated manually. The α-phase is more volatile; it can be resublimed under less extreme conditions and tends to vaporize from a heated finger more readily than the β-phase: dec (β-phase) >350 °C; infrared spectrum (β-phase, 1600–250 cm^{-1} region) 1331 (m), 1307 (s), 1281 (m), 1255 (w), 1247 (w), 1142 (m), 1079 (w), 1068 (w), 919 (w), 805 (w), 796 (w), 750 (m), 733 (m), 688 (vs), 678 (vs), 649 (m), 616 (s), 391 (s) cm^{-1}.

X-ray Measurements. A brass-colored block of the β-phase of **1** was mounted on a glass fiber and coated with epoxy. X-ray data were collected on an ENRAF-Nonius CAD-4 at 293 K with monochromated Mo K_α (λ = 0.71073 Å radiation) to a $2\theta_{max}$ of 23°. A ψ-scan absorption correction varied from 0.58–1.00. The structure was solved using MULTAN and refined by full-matrix least squares which minimized $\sum w(\Delta F)^2$. In the final full-matrix least-squares refinement R = 0.042 for 1346 reflections ($I > 3\sigma(I)$) and 169 parameters (C and N atoms were refined isotropically). H atoms were constrained to idealized positions (C–H = 0.95 Å) with isotropic B values of 1.2 times B_{eq} of the attached C atom. Data collection, structure solution, and refinement parameters are available as supplementary material.

Conductivity Measurements. The conductivity measurements were performed with a Keithley 236 unit. Whereas the needle-like α-phase allowed a reliable four-point-probe bar geometry, the platelet samples of the β-phase were measured with the van der Pauw technique. The resulting error in comparisons between the two phases could be up to a factor of 2 as a result of the geometrical factor. The four contacts were made with gold paint, resulting in a contact resistance that was at least two orders of magnitude higher than the sample resistance. This limited the temperature window of the measurements. The contact resistance decreased on heating the sample, which might be the origin of the scatter in the data points in Figure 6. The carrier density and mobility were calculated by assuming that the carriers were due to thermal activation across the band (intrinsic semiconductor).[7] It should be noted that small errors in the determination of the energy gap propagate exponentially in the derivation of the mobility and carrier density.

Magnetic Susceptibility Measurements. The magnetic susceptibility was measured from 4.2 to 550 K using the Faraday technique. Details of this apparatus have been previously described.[9] The applied field was 14 kOe, and the measured susceptibility was checked for field dependence at several temperatures.

Band Structure Calculations. The band structures were carried out with the EHMACC suite of programs using parameters discussed previously.[8a,10] The off-diagonal elements of the Hamiltonian matrix were calculated with the standard weighting formula.[11]

Acknowledgment. Financial support at Guelph was provided by the Natural Sciences and Engineering Research Council of Canada and at Arkansas by the National Science Foundation (EPSCOR program) and the State of Arkansas.

Supplementary Material Available: Tables of crystal data, structure solution, and refinement (S1), atomic coordinates (S2), bond lengths and angles (S3), and anisotropic thermal parameters (S3) for β-1,3-[$(Se_2N_2C)C_6H_4(CN_2Se_2)$] (7 pages). Ordering information is given on any current masthead page.

(9) (a) DiSalvo, F. J.; Waszczak, J. V. *Phys. Rev.* **1981**, *B23*, 457. (b) DiSalvo, F. J.; Menth, A.; Waszczak, J. V.; Tauc, J. *Phys. Rev.* **1972**, *B6*, 4574.

(10) Basch, H.; Viste, A.; Gray, H. B. *Theor. Chim. Acta* **1965**, *3*, 458.

(11) Ammeter, J. H.; Burghi, H. B.; Thibeault, J. C.; Hoffmann, R. *J. Am. Chem. Soc.* **1978**, *100*, 3686.

Redistribution of Reduced Thiophene Ligands in the Conversion of $(C_5R_5)Rh(\eta^4\text{-}C_4Me_4S)$ to $[(C_5R_5)Rh]_3(\eta^4,\eta^1\text{-}C_4Me_4S)_2$

Shifang Luo, Anton E. Skaugset, Thomas B. Rauchfuss,* and Scott R. Wilson

Contribution from the School of Chemical Sciences, University of Illinois, Urbana, Illinois 61801.
Received July 8, 1991

Abstract: The thermal decomposition of $(C_5Me_5)Rh(\eta^4\text{-}C_4Me_4S)$ (**1**) has been examined by spectroscopic, kinetic, and structural studies. Compound **1** cleanly eliminates free C_4Me_4S to give $[(C_5Me_5)Rh]_3(\eta^4,\eta^1\text{-}C_4Me_4S)_2$ (**2a**). The structure of the analogous compound $[(C_5Me_4Et)Rh]_3(\eta^4,\eta^1\text{-}C_4Me_4S)_2$ (**2b**) consists of a pair of $(C_5Me_4Et)Rh(\eta^4\text{-}C_4Me_4S)$ ligands bound to a central $(C_5Me_4Et)Rh^I$ unit through the sulfur atoms. The conversion of **1** to **2a** occurs via a second-order process (in rhodium) with k(60 °C) = 3.94 × 10^{-4} $M^{-1}\cdot s^{-1}$ which implicates an associative mechanism. Activation parameters are $\Delta H^\ddagger$ = 20.1 ± 0.1 kcal/mol and $\Delta S^\ddagger$ = −13.9 ± 3.1 cal/mol·K. Dynamic ^1H NMR studies demonstrate that **2a** maintains its structure in solution but that it experiences restricted rotation about the two Rh–S bonds. Compound **2a** decomposes via a first-order process with k(100 °C) = 8.94 × 10^{-6} s^{-1} to give $(C_5Me_5)_2Rh_2C_4Me_4S$, **3**.

Introduction

The chemistry of thiophene–metal interactions has been of recent interest with emphasis on structural and reactivity principles.[1] A large number of thiophene complexes has been prepared in recent years, and several bonding modes have been identified.[2] Studies on thiophene complexation have been motivated by intense interest in the molecular mechanisms of the industrially important hydrodesulfurization process (HDS).[3] In HDS liquid fossil fuels are subjected to catalytic hydrogenation conditions with the goal of cleaving the constituent C–S bonds to give a sulfur-free hydrocarbon. Thiophene derivatives are particularly common constituents in fossil fuels[4] and are of special interest because of

(1) Rauchfuss, T. B. *Prog. Inorg. Chem.* **1991**, *39*, 259. Angelici, R. J. *Coord. Chem. Rev.* **1990**, *105*, 61. Angelici, R. J. *Acc. Chem. Res.* **1988**, *21*, 387.

(2) Some recent studies of thiophene complexes: (a) Ganja, E. A.; Rauchfuss, T. B.; Wilson, S. R. *Organometallics* **1991**, *10*, 270. (b) Jones, W. D.; Dong, L. *J. Am. Chem. Soc.* **1991**, *113*, 559. (c) Wang, D.-L.; Hwang, W.-S. *J. Organomet. Chem.* **1991**, *406*, C29. (d) Riaz, U.; Curnow, O.; Curtis, M. D. *J. Am. Chem. Soc.* **1991**, *113*, 1416. (e) Clark, P. D.; Fait, J. F.; Jones, C. G.; Kirk, M. J. *Can. J. Chem.* **1991**, *69*, 590. (f) Choi, M.-G.; Robertson, M. J.; Angelici, R. J. *J. Am. Chem. Soc.* **1991**, *113*, 4005.

(3) Gates, B. C.; Katzer, J. R.; Schuit, G. C. A. *Chemistry of Catalytic Processes*; McGraw-Hill: New York, 1979. Zonnevylle, M. C.; Hoffmann, R.; Harris, S. *Surf. Sci.* **1988**, *199*, 320. Harris, S.; Chianelli, R. R. *J. Catalysis* **1986**, *98*, 17.

(4) *Geochemistry of Sulfur in Fossil Fuels*; Orr, W. L., White, C. M., Eds.; American Chemical Society: Washington, DC, 1990. Galperin, G. D. *Chemistry of Heterocyclic Compounds*; Gronowitz, S., Ed.; John Wiley & Sons, Inc.: New York, 1986; Vol. 44, Part 1, p 325.

0002-7863/92/1514-1732$03.00/0

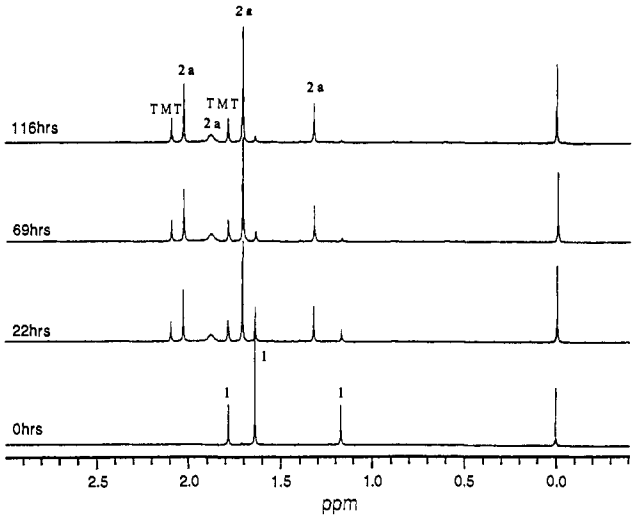

Figure 1. Time course 400-MHz ^1H NMR spectra for the conversion of **1** to **2a**. The peaks for the compounds **1**, **2a**, and C_4Me_4S (TMT) are labeled.

their relative resistance to hydrogenolysis. The diminished reactivity of thiophenic substrates may be related to their weak coordinating properties.[5]

Insights into the mechanism of thiophene desulfurization have come primarily from organometallic models and surface science studies of thiophene on single crystals.[6] One of the most powerful tools in surface science is temperature-programmed desorption (TPD) wherein the thermolysis of a catalyst-absorbed substrate ensemble is monitored by analysis of the small molecule fragments vs time. Analogous to TPD, we have described a series of experiments that involve solution analogues of TPD which entail the monitoring of the thermolysis of preformed metal–thiophene complexes. Two previous studies have focused on the decomposition of bimetallic thiophene derivatives,[7,8] both of which result in desulfurization of the heterocycle. The present work focuses on the thermal decomposition of a highly reduced monometallic thiophene complex.

Results

Solution Properties of $[(C_5Me_5)Rh]_3(\eta^4,\eta^1\text{-}C_4Me_4S)_2$. This study began with the finding that solid samples of $(C_5Me_5)Rh(\eta^4\text{-}C_4Me_4S)$[9] (**1**) slowly decompose to give a new complex $[(C_5Me_5)Rh]_3(\eta^4,\eta^1\text{-}C_4Me_4S)_2$, (**2a**), and free C_4Me_4S. In solution the transformation occurs cleanly over a period of several days at 60 °C to give **2a** and free C_4Me_4S (Figure 1). The yield of **2a** and C_4Me_4S are quantitative based on ^1H NMR spectroscopy. Preparative scale reactions afford **2a** as yellow crystals which are soluble in nonpolar organic solvents. Its solutions are quite air-sensitive and react readily with dry air to give the previously characterized *S*-oxide $(C_5Me_5)Rh(\eta^4\text{-}C_4Me_4SO)$.[10]

Compound **2a** has been characterized by ^1H and ^{13}C NMR spectroscopies, elemental analysis, and in the case of **2b**, single-crystal X-ray diffraction. The ^1H NMR spectrum of **2a** exhibits singlets for the two types of C_5Me_5 groups and a singlet for the 2,5-methyl of the C_4Me_4S groups. A broad feature at 1.88 ppm was assigned to the 3,4-methyl groups of the C_4Me_4S ligand based on our spectrosopic characterization of $[(C_5Me_5)Rh]_3(\eta^4,\eta^1\text{-}3,4\text{-}d_2\text{-}C_4Me_4S)_2$ (**2c**). Except for the smaller of the two C_5Me_5

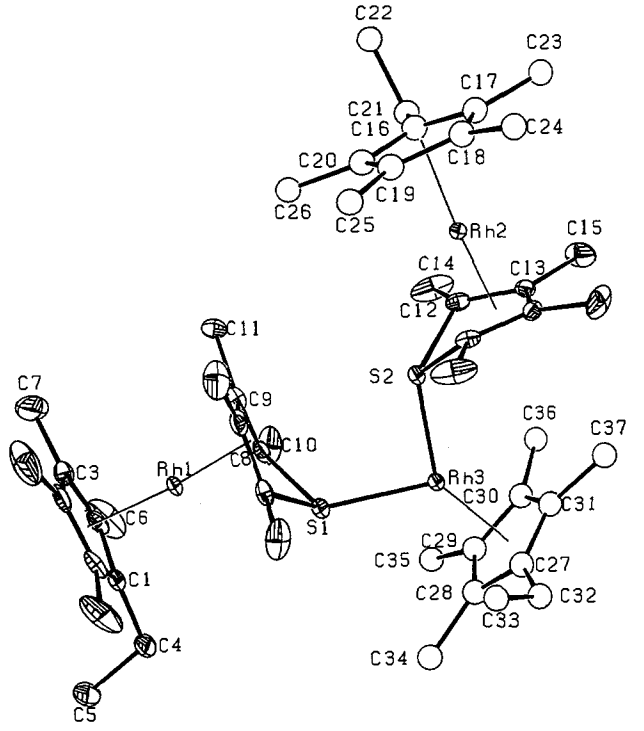

Figure 2. The structure of $[(C_5Me_4Et)Rh(\eta^4,\eta^1\text{-}C_4Me_4S)]_2Rh(C_5Me_4Et)$ with thermal ellipsoids drawn at the 35% probability level.

resonances, all ^1H NMR signals split symmetrically at lower temperatures such that at −70 °C (500 MHz) a 2:2:2:2:5:5:5 pattern was observed. It can also be seen from the ^1H NMR spectra in Figure 1 that **1** is unaffected by the dynamics of **2a**, implicating an intramolecular process. At −70 °C, thirteen of the expected fourteen ^{13}C resonances were observed. These data are collectively consistent with restricted rotation about the Rh–S bonds in **2a**; the stable rotamer features two nonequivalent $(C_5Me_5)Rh(\eta^4\text{-}C_4Me_4S)$ moieties. In the solid-state structure, **2b** exists as an unsymmetrical rotamer (vide infra).

The conversion of **1** to **2** in benzene-d_6 solutions was monitored at various temperatures by ^1H NMR spectroscopy. Excellent mass balance was observed for the conversion of **1** into **2a**, according to eq 1. The rate of disappearance of **1** was found to be sec-

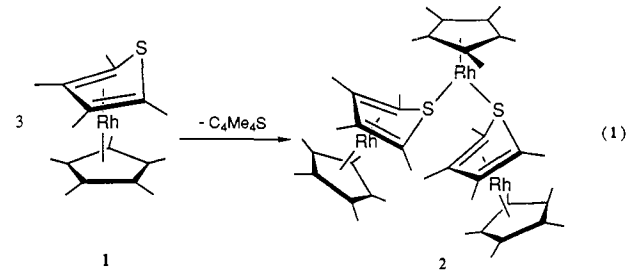

(1)

ond-order in [**1**] based on the linearity of plots of $[\mathbf{1}]^{-1}$ vs time. The temperature dependence of the rate constants provided the following activation parameters: $\Delta H^{\ddagger} = 84.2\ (\pm 4)$ kJ/mol, $\Delta S^{\ddagger} = 58.2\ (\pm 12)$ J/(mol K).

Structure of $[(C_5Me_4Et)Rh]_3(\eta^4,\eta^1\text{-}C_4Me_4S)_2$. Orange crystals of $[(C_5Me_4Et)Rh(\eta^4,\eta^1\text{-}C_4Me_4S)]_2Rh(C_5Me_4Et)$ (**2b**) were examined by X-ray diffraction at −75 °C. The structure consists of a pair of $(C_5Me_4Et)Rh(\eta^4\text{-}C_4Me_4S)$ subunits bound through the axial position of the sulfur atoms to a central $(C_5Me_4Et)Rh$ unit (Figure 2). The whole molecule possesses a symmetry plane which contains S1, Rh3, and S2 atoms and bisects two structurally similar terminal $(C_5Me_4Et)Rh(\eta^4\text{-}C_4Me_4S)$ fragments. The thiophene rings in the molecule are folded such that the S atoms are pointed toward the central Rh3 atom. The dihedral angle is 33.9 (0.2)° between planes defined by C8–C9–C9′–C8′ and C8–S1–C8′ and 33.7 (0.2)° between planes defined by C12–C13–C13′–C12′ and C12–S2–C12′. As a comparison, the

(5) Amarasekera, J.; Rauchfuss, T. B. *Inorg. Chem.* **1989**, *28*, 3875.
(6) Gellman, A. J. *J. Am. Chem. Soc.* **1991**, *113*, 4435 and references therein.
(7) Ogilvy, A. E.; Draganjac, M.; Rauchfuss, T. B.; Wilson, S. R. *Organometallics* **1988**, *7*, 1171 and references therein.
(8) Luo, S.; Ogilvy, A. E.; Rauchfuss, T. B.; Rheingold, A. L.; Wilson, S. R. *Organometallics* **1991**, *10*, 1002.
(9) Ogilvy, A. E.; Skaugset, A. E.; Rauchfuss, T. B. *Organometallics* **1989**, *8*, 2739.
(10) Skaugset, A. E.; Rauchfuss, T. B.; Stern, C. A. *J. Am. Chem. Soc.* **1990**, *112*, 2432.

thiophene folding angle is 42° in $Cp^*Ir(\eta^4\text{-}2,5\text{-}Me_2C_4H_2S)$[11] and 28° in $Cp^*Rh(\eta^4\text{-}C_4Me_4S)$.[9]

Prior to this work, thioether derivatives of the $(C_5R_5)Rh^I$ fragment were unknown.[12] Other examples of rhodium(I) thioether complexes are $[Rh([9]\text{-}aneS_3)(cod)][BF_4]$,[13] $[Rh([9]\text{-}aneS_3)(C_2H_4)_2][BF_4]$,[13] and $[Rh([14]\text{-}aneS_4)]Cl$.[14] The averaged Rh–S distances of 2.216 (6) Å in **2b** is significantly shorter than 2.391 Å in $[Rh([9]\text{-}aneS_3)(cod)][BF_4]$,[13] 2.399 Å in $[Rh([9]\text{-}aneS_3)(C_2H_4)_2][BF_4]$,[13] and slightly shorter than 2.272 Å in $[Rh([14]\text{-}aneS_4)]Cl$.[14] The distances between the terminal Rh and sulfur atoms are 2.918 (9) Å which may be related to the novel donor properties of the $\eta^4\text{-}C_4Me_4S$ ligand as the sum of the van der Waals distances between Rh and S is 3.195 Å.[15] The solid-state structure is consistent with the low-temperature ^1H NMR spectrum of **2a**.

Thermal Decomposition of $[(C_5Me_5)Rh]_3(\eta^4,\eta^1\text{-}C_4Me_4S)_2$. The thermolysis of **2a** was found to occur over the course of several days at 100 °C. The rate of the decomposition of **2a** is first-order but somewhat complex. At 100 °C we observed the formation of free C_4Me_4S, small amounts of **1**, the new compound **3**, and other unidentified species. Traces of **3** are also evident in the final stages of the conversion of **1** to **2a** (Figure 1). A small amount of this green compound **3** was obtained after multiple recrystallizations of the residue obtained from the thermolysis of $(C_5Me_5)Rh(\eta^4\text{-}C_4Me_4S)$ in toluene at 120 °C. Its FDMS indicates the formula $[(C_5Me_5)Rh]_2(C_4Me_4S)$. Its ^1H NMR spectrum consists of two equally intense C_5Me_5 signals and four methyl singlets. On the basis of the spectroscopic data and its stoichiometric similarity to $[(CO)_3Fe]_2SC_4R_4$,[7,16] **3** is assigned the structure shown in eq 2.

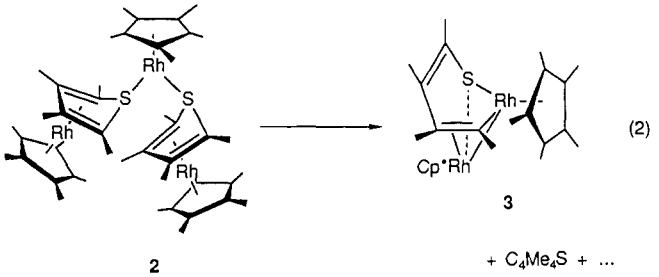

Discussion

Previously we have shown that two-electron reduction of $[(C_5Me_5)Rh(\eta^5\text{-}C_4Me_4S)]^{2+}$ produces $(C_5Me_5)Rh(\eta^4\text{-}C_4Me_4S)$ (**1**).[9] The reduction causes the thiophene ring to fold concomitant with cleavage of the Rh–S bond. The uncoordinated sulfur atom in the reduced product is an excellent donor site which promotes the attachment of a second metal to the thiophene ligand which in turn facilitates C–S cleavage.

The electron-rich character of the S atom[10,17] in $\eta^4\text{-}C_4R_4S$ ligands sharply contrasts with the weak nucleophilicity and basicity of the free heterocycles and the $\eta^5\text{-}C_4R_4S$ ligands. The high nucleophilicity and basicity of the $\eta^4\text{-}C_4R_4S$ ligands may result from repulsive interactions between the nonbonding electrons on Rh and S.[18] In **2b**, the nonbonding Rh···S distances are 2.92 Å, only 20% longer than conventional Rh–S bonds. A comparable repulsive interaction between the nonbonding electrons on the metal and an adjacent main group center has also been invoked to explain the high nucleophilicity of the sulfur center in $CpRu(PR_3)_2SR$.[5]

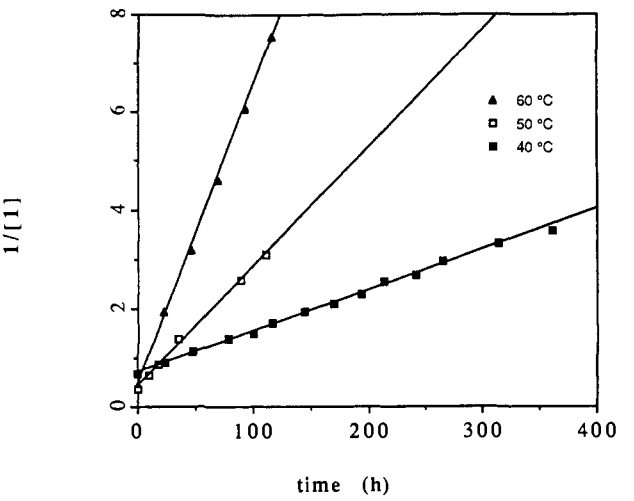

Figure 3. Second-order kinetics plots of $[1]^{-1}$ vs time (h) for various temperatures.

The kinetic data indicate that **1** converts to **2** via an associative process. The negative activation entropy is also consistent with an associative mechanism. Given the high nucleophilicity of the sulfur center in **1**, the conversion is likely initiated by attack of the sulfur atom at the metal center of a second molecule of **1**. This initial event in the conversion of **1** to **2a** requires the intermediacy of $[(C_5Me_5)Rh(C_4Me_4S)]_2$. In such a species an 18e configuration can be maintained about each metal center only if there is a change in the hapticity of either C_5Me_5 or C_4Me_4S ligands. Our experiments do not distinguish these possibilities. Basolo has suggested the η^5- to η^3-slippage of the cyclopentadienyl ring to explain the associative mechanism of the substitution reactions of $(C_5H_5)Rh(CO)_2$.[19] It has also been reported that the substitution reactions of $(C_5H_5)Rh(C_2H_4)_2$ with phosphines and phosphites also are associative.[20] In the latter case the presence of the ethylene ligands requires that the hapticity change be localized on the C_5H_5 ligand, since the ethylene ligands would irreversibly dissociate otherwise. The similarity of the metal coordination spheres in **1** and $(C_5H_5)Rh(C_2H_4)_2$ suggests that the conversion of **1** to **2** proceeds via $[(\eta^5\text{-}C_5Me_5)Rh(\eta^4,\eta^1\text{-}C_4Me_4S)][\eta^3\text{-}C_5Me_5)Rh(\eta^4\text{-}C_4Me_4S)$. This intermediate could be followed by the coupled set of haptotropic rearrangement to give $[(\eta^5\text{-}C_5Me_5)Rh(\eta^4,\eta^1\text{-}C_4Me_4S)][\eta^5\text{-}C_5Me_5)Rh(\eta^2\text{-}C_4Me_4S)]$, which in turn reacts further with **1** to produce **2**.

On the basis of our previous study on $(C_5Me_5)Rh\{(\eta^4,\eta^1\text{-}C_4Me_4S)Fe(CO)_4\}$[8] and this study, it follows that the equilibrium metal/thiophene stoichiometry depends on the oxidation state of the metal. While the equilibrium $(C_5Me_5)Rh^{III}/C_4Me_4S$ ratio is 1:1 as found in $[(C_5Me_5)Rh(\eta^5\text{-}C_4Me_4S)]^{2+}$, the $(C_5Me_5)Rh^I/C_4Me_4S$ ratio is 3:2 as found **2**. This change reflects the strong tendency of the η^4-thiophene ligands to more fully utilize their complement of nonbonding electrons. For this reason $\eta^4,\eta^1\text{-}C_4R_4S$ ligands are far more likely to exist on multimetallic catalysts than are $\eta^4\text{-}C_4R_4S$ ligands. It is therefore significant that both this and our previous system[8] show that $\eta^4,\eta^1\text{-}C_4R_4S$ coordination leads to C–S cleavage.

Experimental Section

Experimental protocols and the preparations of starting materials were described previously.[8] ^1H NMR spectra were obtained on a Varian Unity spectrometer (400 MHz) and General Electric spectrometers (QE-300 and GN-500 MHz).

Kinetics Studies. A 5-mm NMR tube containing benzene-d_6 solution of **1** with internal tetramethylsilane standard was subjected to three freeze–pump–thaw cycles and flame sealed. The tubes were stored in a thermostated oven (ca. ±0.5 °C) and removed only for several minutes for recording the spectra. The signal corresponding to the 2,5-methyl of **1** was integrated vs the TMS signal (Figure 3). Plots of the appearance

(11) Chen, J.; Angelici, R. J. *Organometallics* **1989**, *8*, 2277.
(12) Russell, M. J. H.; White, C.; Yates, A.; Maitlis, P. M. *J. Chem. Soc., Dalton Trans.* **1978**, 849.
(13) Blake, A. J.; Halcrow, M. A.; Schröder, M. *J. Chem. Soc., Chem. Commun.* **1991**, 253.
(14) Yoshida, T.; Ueda, T.; Adachi, T.; Yamamoto, K.; Higuchi, T. *J. Chem. Soc., Chem. Commun.* **1985**, 1137.
(15) *The Elements*; Emsley, J., Ed.; Oxford University Press: New York, 1989.
(16) LeBorgne, G.; Grandjean, D. *Acta Crystallogr.* **1977**, *B33*, 344. Hübener, P.; Weiss, E. *J. Organomet. Chem.* **1977**, *129*, 105.
(17) Chen, J.; Angelici, R. J. *Organometallics* **1990**, *9*, 849.
(18) Harris, S., private communication.
(19) Schuster-Woldan, H. G.; Basolo, F. *J. Am. Chem. Soc.* **1966**, *88*, 1657.
(20) Cramer, R.; Seiwell, L. P. *J. Organomet. Chem.* **1975**, *92*, 245.

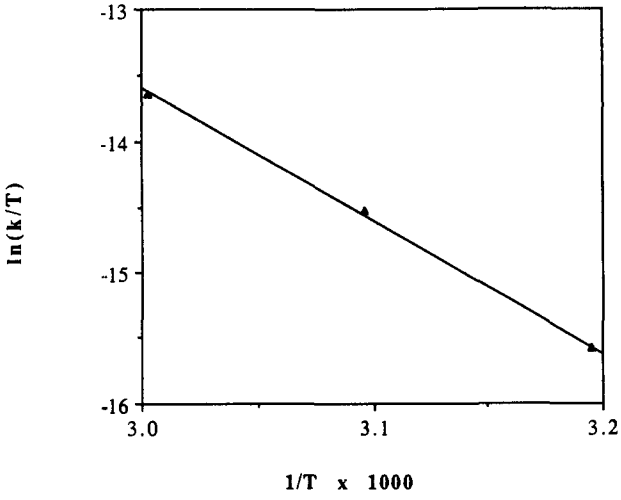

Figure 4. Plot of ln (k/T) vs $1/T$ (×1000) for the conversion of **1** to **2a**.

of **2a** also obeyed second-order kinetics. The absolute concentration of $[1]_0$ for the calculation of rate constants was obtained by calculating the ^{1}H NMR integration of 2,5-methyl groups of **1** vs the internal TMS standard of known concentration. Following the Eyring equation, ln (k/T) were plotted vs $1/T$ (Figure 4).

$[(C_5Me_5)Rh]_3(\eta^4,\eta^1\text{-}C_4Me_4S)_2$. A Pyrex tube containing 0.260 g of **1** (0.687 mmol) and 15 mL of benzene was flame-sealed and placed in a thermostated oven and kept at 60 °C for 5 days. The tube was opened inside a dry box and a deep red yellow solution was transferred to a 100-mL Schlenk flask. The yield is quantitative after removal of volatiles under high vacuum. An analytically pure sample was obtained by dissolving the sample in hexane followed by concentration and cooling to −20 °C. ^{1}H NMR (C_6D_6, 20 °C) 2.03 (s, 15 H), 1.88 (br, s, 12 H), 1.71 (s, 30 H), 1.32 (s, 12 H); ^{1}H NMR ($C_6D_5CD_3$, −70 °C) 2.14 (s, 15 H), 1.93 (s, 6 H), 1.80 (s, 6 H), 1.74 (s, 15 H), 1.73 (s, 15 H), 1.39 (s, 6 H), 1.38 (s, 6 H); ^{13}C NMR (C_6D_6, 20 °C, $J(^{13}C, ^{103}Rh)$) 93.43 (d, 5.5), 92.72 (d, 4), 86.42 (br), 12.81 (s), 12.06 (s), 11.46 (s), 9.75 (s). ^{13}C NMR ($C_6D_5CD_3$, −70 °C, $J(^{13}C, ^{103}Rh)$): 93.21 (unres), 93.07 (unres), 92.43 (d, 2.5), 86.36 (d, 3.63), 85.62 (d, 5.3), 58.66 (d, 15.8), 53.21 (d, 14.1), 13.10 (s), 12.86 (s), 12.33 (unres s), 11.87 (s), 9.89 (s). Anal. Calcd for $C_{46}H_{69}Rh_3S_2$: C, 55.53; H, 6.99; S, 6.44. Found: C, 55.63; H, 7.16; S, 5.91. $[(C_5Me_4Et)Rh]_3(\eta^4,\eta^1\text{-}C_4Me_4S)_2$ (**2b**) and $[(C_5Me_5)Rh]_3(\eta^4,\eta^1\text{-}3,4\text{-}d_2\text{-}C_4Me_4S)_2$ (**2c**) were prepared via the same method starting from $(C_5Me_4Et)Rh(\eta^4\text{-}C_4Me_4S)$ and $(C_5Me_5)Rh(\eta^4\text{-}3,4\text{-}d_2\text{-}C_4Me_4S)$, respectively.

$(C_5Me_5)_2Rh_2SC_4Me_4$, 3. NMR analysis of the thermolysis of a toluene solution of **2a** indicates that **3** forms in ca. 35% yield. A solution of 0.286 g of **1** in 10 mL of toluene was heated to reflux for 24 h. After removal of solvent, the solid product was recrystallized five times from hexane to afford a small amount of analytically pure dark green microcrystals. The yield was ca. 10%. The low yield is due to the loss of the product in the recrystallization process. ^{1}H NMR (C_6D_6) 2.56 (s, 3 H), 1.89 (s, 15 H), 1.82 (s, 3 H), 1.74 (s, 3 H), 1.70 (s, 15 H), 1.47 (s, 3 H); FDMS m/e 616 (M^+), 308 (M^{2+}). Anal. Calcd for $C_{28}H_{42}Rh_2S$: C, 54.55; H, 6.89; S, 5.20. Found: C, 55.50; H, 7.22; S, 5.20.

Crystallographic Determination of $[(C_5Me_4Et)Rh(\eta^4,\eta^1\text{-}C_4Me_4S)]_2Rh(C_5Me_4Et)$. The orange crystal of **2b** was grown by slow evaporation of a toluene solution of $(C_5Me_4Et)Rh(\eta^4\text{-}C_4Me_4S)$ at ca. 35 °C. The crystal was mounted using Paratone-N oil (Exxon) to a thin glass fiber and then cooled to −75 °C. Unit cell parameters were obtained by a least-squares fit to the automatically centered settings for 15 reflections ($22.0° < 2\Theta < 24.4°$). The space group was determined by the average values of the normalized structure factors and successful refinement of the proposed model. The choice of the alternative space group $P2_1$ did not lead to improvements in the structure. Numerical absorption correction was applied to the data set with maximum and minimum transmission factors of 0.764 and 0.692, respectively. The structure was solved by direct methods (SHELXS-86). Correct positions for the rhodium and sulfur atoms were deduced from an E-map. Subsequent least-squares difference Fourier calculations revealed positions for the remaining non-hydrogen atoms. Two of the three C_5Me_5 rings were disordered about the crystallographic mirror. Hydrogen atoms were not included in the structure factor calculations. In the final cycle of least squares a common isotropic thermal parameter was varied for the disordered C_5Me_5 carbon atoms, and anisotropic thermal coefficients were refined for the remaining atoms. Successful convergence was indicated by the maximum shift/error for the last cycle. The highest peaks in the final difference map were in the vicinity of the disordered C_5Me_5 rings. A final analysis of variance between observed and calculated structure factors showed an inverse dependence on sin (θ). Selected bond distances and angles are listed in Table I. Crystal data collection and refinement parameters are listed in Table II.

Table I. Selected Bond Distances (Å) and Angles (deg) for **2b**

	(a) Bond Distances		
Rh1–C8	2.128 (6)	Rh1–C9	2.095 (6)
Rh2–C12	2.128 (6)	Rh2–C13	2.095 (6)
Rh3–S1	2.221 (2)	Rh3–S2	2.212 (2)
S1–C8	1.802 (7)	S2–C12	1.815 (6)
C8–C9	1.415 (9)	C12–C13	1.423 (9)
C9–C9	1.439 (10)	C13–C13	1.422 (9)
	(b) Bond Angles		
S1–Rh3–S2	92.53 (8)	C8–S1–C8	82.1 (3)
Rh3–S1–C8	120.7 (2)	C12–S2–C12	81.4 (3)
Rh3–S2–C12	119.6 (2)	C9–C8–S1	112.0 (5)
C13–C12–S2	112.2 (4)	C8–C9–C9	109.2
C12–C13–C13	109.4 (5)		

Table II. Summary of Crystallographic Data for **2b**

formula	$C_{49}H_{75}S_2Rh_3$
crystal system	monoclinic
space group	$P2_1/m$
a, Å	11.215 (2)
b, Å	15.187 (4)
c, Å	14.630 (3)
β, deg	107.87 (2)
Z	4
density (calc), g/cm^{-3}	1.452
color	orange
dimensions, mm	0.1 × 0.3 × 0.3
temp, K	198
diffractometer	Enraf-Nonius CAD4
μ, cm^{-1}	11.31
transmission factor range	0.692–0.764 (numerical)
2θ limit, deg	2.0–38.0 $(+h+k\pm l)$
	38.0–48.0
no. of reflcn measd	4180
no. of unique reflcns	3867
no. of reflcns with $I > 2.58\sigma(I)$	3229
R	0.045
R_w	0.062
$\Delta(\rho)$, eÅ^{-3}	1.00

Acknowledgment. This research was supported by the Department of Energy. We thank Ann Ogilvy and Eric Houser for experimental assistance.

Registry No. 1, 123307-89-1; **2a**, 138407-52-0; **2b**, 138407-55-3; **2c**, 138407-56-4; **3**, 138407-53-1; $(C_5Me_4Et)Rh(\eta^4\text{-}C_4Me_4S)$, 125666-56-0; $(C_5Me_5)Rh(\eta^4\text{-}3,4\text{-}d_2\text{-}C_4Me_4S)$, 138407-54-2.

Supplementary Material Available: Tables of atomic coordinates and isotropic thermal parameters, bond distances and angles, and positional and thermal parameters (6 pages); table of observed and calculated structure factors (14 pages). Ordering information is given on any current masthead page.